Available online at www.sciencedirect.com
SCIENCE DIRECT®
Journal of Electroanalytical Chemistry 548 (2003) 85–94
Journal of Electroanalytical Chemistry
www.elsevier.com/locate/jelechem

Convective mass transfer to partially recessed and porous electrodes

Elisabet Ahlberg [a,*], Fredrik Falkenberg [a], José A. Manzanares [b], David J. Schiffrin [c]

[a] Department of Chemistry, University of Göteborg, S-412 96 Goteborg, Sweden
[b] Department of Thermodynamics, University of Valencia, E-46100 Burjassot, Spain
[c] Department of Chemistry, University of Liverpool, Liverpool L69 7ZD, UK

Received 7 January 2003; received in revised form 13 March 2003; accepted 23 March 2003

Abstract

The diffusional problem of a rotating porous electrode has been analysed based on the mass transfer equations for a partially blocked electrode. It is shown that the porous geometry leads to a dependence of the current on rotation rate identical to that corresponding to a coupled diffusion-activated electron transfer mechanism. The apparent rate constant, however, is related only to the geometry of the porous surface. It is shown that the characteristic diffusional length corresponds to the pore dimension modified by a term including the transition from linear to spherical diffusional geometry at the pore entrance. The theory is compared with experimental results for the reduction of hexacyanoferrate(III) and oxygen on platinum electrodes covered by an insulating film of nickel hydroxide. It is shown that the limiting currents from Koutecký–Levich plots give a much larger blocking factor than that derived from the analysis of a semilogarithmic current function. A comparison of these two methods for calculating the blocking factor provides information on the tortuosity coefficient of the film.

Keywords: Partially blocked recessed electrode; Porous Pt/Ni(OH)$_2$ electrode; Rotating disc electrode; Tortuosity; Oxygen reduction; Electrochemical kinetics

1. Introduction

The kinetics of interfacial electron transfer reactions are intimately coupled to the rates of diffusion and migration of reactants and/or products, since both determine reactive species surface concentrations. The latter are required for the elucidation of reaction mechanisms and for this reason, there has been a great deal of effort to find appropriate electrode geometries where the diffusion problem is well defined. However, electrode surfaces are often heterogeneous and, for example, adsorption or oxide formation result in the establishment of non-linear diffusion conditions that can profoundly affect the calculated rate constant derived from the measured current–potential relationships.

If the sites of electron transfer are discrete, i.e. the electrode is partially blocked, the diffusional field close to the surface can be hemispherical or a combination of hemispherical and linear geometries [1–3]. For transient techniques, the time scale of the experiment determines whether behaviour as an array of ultramicroelectrodes or that of a planar electrode is observed [4,5]. The electrochemical rate constants calculated from cyclic voltammetry are strongly influenced by these surface geometry considerations [6,7] and similar effects have been observed using techniques such as chronopotentiometry and chronoamperometry [7–10].

Although the non-linear diffusional effects resulting for the partial blocking of an electrode surface have been extensively considered [4,5,11–13], the important practical case of electrochemical reactions at partially blocked and recessed electrodes has not received much attention. For instance, transient mass transfer at a coated RDE has been considered by Deslouis et al. [14]. Geometry consisting of an array of recessed electrodes is commonly found when the electrode is covered by an insulating or poorly conducting film. In this case, the diffusional field established under convective conditions in the solution close to the insulating film surface cannot

* Corresponding author. Tel.: +46-31-772-2879; fax: +46-31-772-2853.
E-mail address: elisabet.ahlberg@inoc.gu.se (E. Ahlberg).

0022-0728/03/$ - see front matter
doi:10.1016/S0022-0728(03)00227-4

be regarded as linear due to the inevitable edge effects at the opening of the pores. Similar effects are present on blocked electrodes and the mass transfer conditions for this geometry have been approximated by Landsberg and co-workers [11–13,15] to the solution of a conductivity problem originally solved by Smythe [16]. The approach consists in replacing the three-dimensional diffusional field by diffusion taking place in cylinders into which all the flux to a particular active centre is confined. This method has been favourably compared with simulations of concentration profiles within the diffusion layer [17]. An analysis of the current response for a recessed electrode in the presence of convective flow has been presented by Girault and co-workers [18]. The aspect ratio of the geometry considered was very different from that considered in the present work since these authors analysed shallow recesses.

A comparison of the two geometries considered in the present work is shown in Fig. 1. Fig. 1a corresponds to a partially blocked rotating disc electrode (RDE), when the height of the pores is $d = 0$. For a recessed RDE (Fig. 1b), the limiting currents extrapolated to infinite rotation rate will give an apparent value of the electron transfer rate constant independent of the potential although the reaction at the electrode surface is diffusionally controlled. This is due to the linear diffusion conditions that are established within the pores as the thickness δ of the diffusion boundary layer (DBL) decreases with increasing rotation rate. For a reversible reaction, in the limit when $\delta \to 0$, the current reaches a constant value determined by linear diffusion within the pores for a concentration at their entrance equal to the bulk concentration of the electroactive material. Thus, even though the reaction is reversible, a Koutecký–Levich (K–L) analysis [19] will lead to an apparent mixed kinetic-diffusional mechanism. The values of the apparent rate constant calculated from RDE experiments will depend, therefore, on both the geometry of the electrode surface and on the electrochemical rate constant rather than only on the kinetics of the interfacial electron transfer reaction.

The purpose of the present work was to find an approximate solution to the diffusional problem for the geometry described in Fig. 1b, taking into account the non-uniformity of the diffusional field close to the electrode surface.

2. Theory

A reduction reaction at a recessed electrode will be considered. The diffusional problem to the electrode surface will be described for the reversible and irreversible reaction cases. First, a simplified flux distribution ignoring the details of the divergence of the flux close to the pore opening will be presented. Then, an approach that takes into account the flux geometry described schematically in Fig. 2 will be worked out based on previous work by Landsberg and co-workers [11–13], and finally, the application of the RDE technique for obtaining parameters describing diffusion in porous electrodes will be discussed.

2.1. Matching linear diffusional fields

For the first case, the geometry described in Fig. 1b will be considered. The electrode is covered by a porous, insulating film of thickness d. The DBL extends from $x = d$ to $d+\delta$, where x is the distance from the electrode surface. For a RDE the thickness of the DBL is given by [19]:

$$\delta = 1.61 D^{1/3} \upsilon^{1/6} \omega^{-1/2} \quad (1)$$

where ω is the rotation rate in rad s^{-1}, D is the diffusion coefficient of the electroactive species and υ is the kinematic viscosity. The use of Eq. (1) for the thickness δ is equivalent to assuming that mass transfer in the DBL is described by a linear diffusion field with no convection.

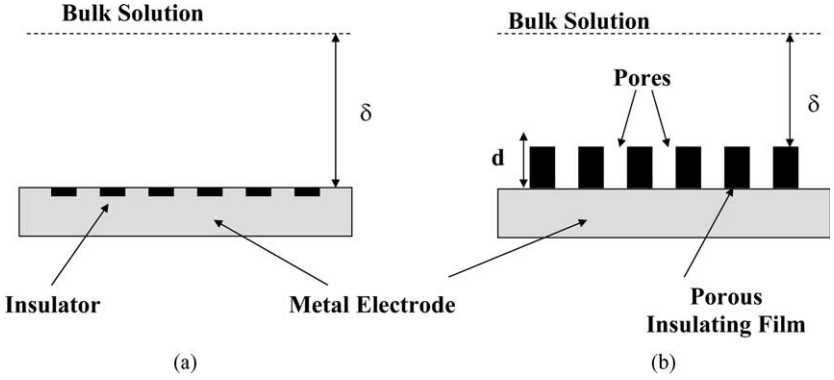

Fig. 1. Schematic representation of (a) a partially blocked and (b) a partially recessed electrode surface under convective flow conditions. δ is the thickness of the diffusional layer and d is the length of the pores.

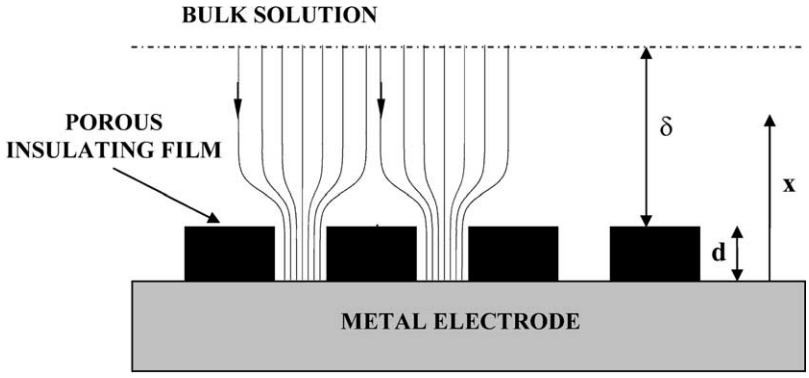

Fig. 2. Schematic diagram of the lines of flux towards a pore showing the linear diffusional field within the pore and pore entrance effects.

The diffusional field must also be linear within the pores because there is no source or sink within them and the boundary condition at their bottom requires that the lines of flux must be perpendicular to the electrode surface. Thus, linear diffusion conditions prevail throughout the system, except at the vicinity of the pore entrance $x = d$, where a discontinuity in the flux density arises due to the difference in cross sectional areas of the pore and the DBL. The question that has to be considered next is what is the limiting current due to mass transfer limitations in this system. For unblocked electrodes, the limiting current due to mass transfer control in the DBL is

$$I_D = -nFAD\frac{c^b}{\delta} \tag{2}$$

where A is the geometrical electrode area and c^b is the bulk concentration of the electroactive species. It is to be expected that porous electrodes will also show this limiting current when the porosity is very high.

In the opposite case of very low porosity electrodes, diffusion across the porous film would be the mass transfer rate-determining step, and the limiting current would be given by:

$$I_s = -nFA_sD\frac{c^b}{d} \tag{3}$$

where A_s is the exposed electrode area at the bottom of the pores.

In the case of mixed DBL-porous film control, the diffusion limiting current must be obtained from the continuity equation by matching the linear diffusion fields. The electric current associated with diffusion in the DBL and inside the pores can be approximated, respectively, by

$$I = -nFAD\left.\frac{\partial c}{\partial x}\right|_{x=d+\delta} = -nFAD\frac{c^b - c(d)}{\delta} = I_D\left[1 - \frac{c(d)}{c^b}\right] \tag{4}$$

$$I = -nFA_sD\left.\frac{\partial c}{\partial x}\right|_{x=0} \approx -nFA_sD\frac{c(d)}{d} = I_s\frac{c(d)}{c^b} \tag{5}$$

where I_D and I_s are the linear diffusional currents to areas A and A_s, respectively, and $c(d)$ is the concentration of the electroactive species at the pore entrance. Mass conservation under steady-state conditions requires the rate of mass transfer to be constant, and Eqs. (4) and (5) then lead to:

$$c(d) = c^b\frac{Ad}{Ad + A_s\delta} = c^b\frac{I_D}{I_D + I_s} \tag{6}$$

and

$$I = I_{Ds} = \frac{I_DI_s}{I_D + I_s} = -nFA_sD\frac{c^b}{d + \delta(A_s/A)} \tag{7}$$

The diffusional current I_{Ds} is defined for convenience; this is the total diffusional current that would be observed for the geometry shown in Fig. 1b. As expected, Eq. (7) reduces to Eqs. (2) and (3) in the limiting cases $\delta A_s/A \gg d$ (very high porosity) and $\delta A_s/A \ll d$ (very low porosity), respectively. From Eq. (7), the equivalent to the K–L equation [10] is now given by:

$$\frac{1}{I} = \frac{1}{I_{Ds}} = \frac{1}{I_s} + \frac{1}{I_D} = -\frac{d}{nFA_sDc^b} - \frac{1.61\upsilon^{1/6}}{nFAD^{2/3}c^b}\frac{1}{\omega^{1/2}} \tag{8}$$

Eq. (8) shows two interesting features. Firstly, the slope of a plot of I^{-1} as a function of $\omega^{-1/2}$ will give a slope identical to that expected for a reversible or irreversible electron transfer reaction, irrespective of whether the surface is partially blocked and recessed or not. Thus, a calculation of the value of nDc^b does not give an indication of the presence of a recessed electrode surface. The value of the K–L slope is not diagnostic of the diffusional geometry close to the electrode surface. Secondly, a finite intercept of the values of I^{-1} extrapolated to $\omega \to \infty$ ($I_D^{-1} \to 0$) is predicted for a reversible reaction and this is related to the value of the ratio d/A_s. Although an apparent activated electron transfer current or an apparent chemical limiting step will be observed, this is unrelated to the kinetics of the

electron transfer reaction but is related to diffusional geometry that is unaffected by the convective mass transfer coefficient outside the pores.

The above simplistic analysis is presented to introduce the ideas that are needed in the rest of the paper.

2.2. Pore entrance geometry effects

The flux geometry for the porous electrode model under convective mass transfer conditions employed is described schematically in Fig. 2 and assumes, as before, the matching of fluxes into the pore and across the DBL. In this case, however, the more accurate description of mass transfer to a partially blocked electrode is employed [11–13]. The main approximation is to consider that the concentration at the top of a pore is constant, independent of the distance measured from the centre of the pore to its edges. This boundary condition applies strictly at the bottom of the pore since the electrode surface is an equipotential and its applicability will be discussed later on. Certainly, the use of a plane from which the effective concentration can be regarded as constant and from which the flux equations for a blocked electrode can be applied greatly simplifies the treatment of the complex diffusional geometry of a porous electrode under convective mass transfer conditions.

The theoretical treatment developed by Landsberg and co-workers [11–13] will be briefly described first and then its transposition to the case of the rotating porous electrode will be presented. Landsberg modelled the diffusional problem of a partially blocked electrode (see Fig. 1a) by considering that the diffusional field between the metal electrode and the limit of the DBL at a distance δ from the surface can be regarded as identical to the solution of the problem of the electrical conductivity between two circular plates of different radii confined by a cylindrical envelope and having a radius equal to the largest of the two contacts. This problem was solved by Smythe in 1953 [16].

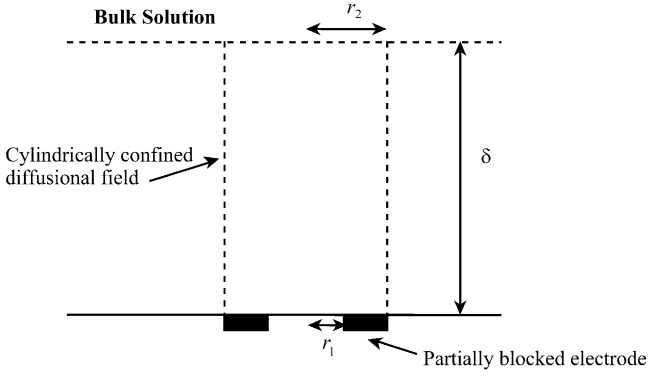

Fig. 3. Diagram of the cylindrically confined diffusional field used showing the dimensions of the two circular areas defining the geometry employed.

The geometry being considered here is shown in Fig. 3. The exposed electrode area A_s at the bottom of the pores is described as a number N_{pore} of disks of radius r_1, so that $A_s = N_{pore}\pi r_1^2$. Similarly, the geometrical surface area A is described as composed of N_{pore} disks of radius r_2, so that $A = N_{pore}\pi r_2^2$. All the lines of flux within each one of the cylindrical pores of radius r_2 and length δ end in the disk of radius r_1 on the electrode surface (see Fig. 2). The relation between the radii r_1 and r_2 and the blocking factor ϕ is then given by:

$$\phi = 1 - \frac{A_s}{A} = 1 - \frac{r_1^2}{r_2^2} \tag{9}$$

This factor represents the fraction of the geometrical surface that is *not* accessible to the electroactive species. These simple geometrical considerations allow the modelling of properties depending on quantities that have a clear physical meaning such as the degree of blocking of the electrode surface.

For a reduction reaction, when the surface concentration is zero, the above model for the partially blocked electrode leads to a relationship between the limiting current and the rotation rate given by [13]:

$$\frac{1}{I} = -\frac{\delta + \Sigma}{nFADc^b} \tag{10}$$

with Σ given by:

$$\Sigma = \sum_n \left| A_n \tanh\left(\frac{x_n \delta}{r_2}\right) \right| \tag{11}$$

where A_n are the coefficients introduced originally by Smythe [16] and given by:

$$A_n = -\frac{r_2}{x_n^2 J_0^2(x_n)} \left\{ \left[\frac{r_2}{r_1} - \left(\frac{r_1}{r_2}\right)^{2.5} \right] \sin\left(x_n \frac{r_1}{r_2}\right) + 2\left(\frac{r_1}{r_2}\right)^{2.5} J_1\left(x_n \frac{r_1}{r_2}\right) \right\} \tag{12}$$

x_n are the zeros of the Bessel function of order 1 $J_1(x)$, and $J_0(x)$ is the Bessel function of order 0.

When this model is transposed to the case of a recessed electrode, the concentration c^b in Eq. (10) must be replaced by $[c^b - c(d)]$. The continuity condition requires that the current I in Eq. (5) must be equal to that in Eq. (10). Therefore,

$$c(d) = c^b \frac{Ad}{Ad + A_s(\delta + \Sigma)} = c^b \frac{Ad}{Ad_{eff} + A_s\delta} \tag{13}$$

and

$$\frac{1}{I} = \frac{1}{I_{Ds}} = \frac{1}{I_s} + \frac{1}{I_D} = -\frac{d_{eff}}{nFA_sDc^b} - \frac{1.61\upsilon^{1/6}}{nFAD^{2/3}c^b} \frac{1}{\omega^{1/2}} \tag{14}$$

where d_{eff} is an effective pore length that takes into account pore entrance effects and is given by $d_{eff} = d +$

$(1-\phi)\Sigma$. When comparing this confined cylindrical model with a linear diffusion approximation (Eqs. (14) and (8), respectively) it is noteworthy that the only result of including pore entrance effects is to change the effective length of the pore from d to d_{eff}. Since Σ is a positive quantity, the pore entrance effects are equivalent to *increasing* the pore length. The above arguments are an approximation since it is implicitly assumed that there is no radial concentration gradient for $x \leq d$.

In addition, it is noteworthy that the K–L slope in Eq. (14) is independent of the electrode area available for electrochemical reactions. The reason for this can be understood with reference to Fig. 2. Provided the variations of δ are comprised within the region where the diffusional field is linear, the dependence of I^{-1} on $\omega^{-1/2}$ will follow the classical Levich relationship.

When the distance between pores is less than the thickness of the DBL, i.e. $2r_2 < \delta$, Σ is given by [13]:

$$\Sigma \approx \sum_n |A_n| \tag{15}$$

Values of $(1/r_2)\Sigma_n A_n$ have been calculated by Landsberg and co-workers [13] and a good non-linear regression fit was obtained for these data using a double exponential function [20]:

$$\frac{1}{r_2}\sum_n |A_n| \approx -0.0314 + 7.632 \times e^{-5.263(r_1/r_2)} + 31.757 \times e^{-25.82(r_1/r_2)} \tag{16}$$

The maximum error in this function was 0.02 for any value of (r_1/r_2). The dependence of the parameter Σ on the number of pores per unit geometrical area, $\Gamma_{\text{pore}} = N_{\text{pore}}/A = 1/\pi r_2^2$, and on the blocking factor ϕ can be calculated from Eqs. (9) and (16) to give:

$$\Sigma \approx \Gamma_{\text{pore}}^{-1/2}\{-0.0177 + 4.306 \times e^{-5.263(1-\phi)^{1/2}} + 17.917 \times e^{-25.82(1-\phi)^{1/2}}\} \tag{17}$$

Fig. 4 shows the dependence of Σ on the blocking fraction for electrode surfaces having different pore densities. This figure shows that, as the pore density Γ_{pore} increases, the correction to the value of d decreases. These results provide guidelines for the analysis of polarisation curves for rotating porous disk electrodes.

The condition for which Eq. (15) is valid ($\delta > 2r_2$) introduces a constraint to the range of rotation rates that can be used for this analysis. For example, the value of δ for $\omega = 2\pi \times 2400$ rpm is $\sim 1.3 \times 10^{-3}$ cm (Eq. (1) with $D = 2 \times 10^{-5}$ cm^2 s^{-1}). Eq. (16) is valid for $2r_2 < \delta$, and for this rotation rate, the minimum surface density of pores for which this analysis is applicable is:

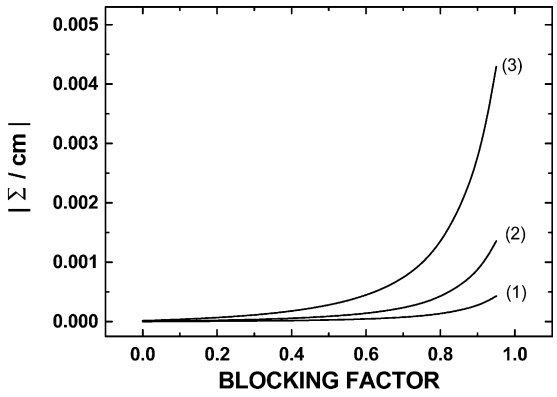

Fig. 4. Dependence of Σ on the blocking fraction for different values of the surface pore density Γ_{pore}: (1) 10^7 cm^{-2}, (2) 10^6 cm^{-2} and (3) 10^5 cm^{-2}.

$$\Gamma_{\text{pore}} = \frac{1}{\pi r_2^2} = \frac{4}{\pi \delta^2} = 7.8 \times 10^5 \text{ cm}^{-2} \tag{18}$$

2.3. Irreversible reactions

Eq. (14) corresponds to a reversible reaction with a surface concentration of zero at the bottom of the pore. The irreversible reaction case can be easily solved by using the mass transfer continuity condition:

$$I = -nFA_s D\frac{c(d) - c(0)}{d} = -nFA_s c(0)k \tag{19}$$

where $c(0)$ is the concentration of the electroactive species at the bottom of the pore, $k(E) = k^0 e^{-\alpha nf(E-E^0)}$ is the electrochemical rate constant, k^0 is the standard rate constant, α is the transfer coefficient, $f = F/RT$, R is the gas constant, T is the absolute temperature, E is the potential and E^0 is the standard potential for the electrochemical reaction.

From the continuity condition, the current I in Eq. (19) must be equal to that in Eq. (10), with c^b replaced by $[c^b - c(d)]$. It is then easy to show that:

$$\frac{1}{I} = \frac{1}{I_k} + \frac{1}{I_{Ds}} = \frac{1}{I_k} + \frac{1}{I_s} + \frac{1}{I_D} = -\frac{1}{nFA_s c^b k} - \frac{d_{\text{eff}}}{nFA_s D c^b} - \frac{1.61\upsilon^{1/6}}{nFAD^{2/3}c^b}\frac{1}{\omega^{1/2}} \tag{20}$$

where $I_k = nFA_s c^b k(E)$ is the kinetic current at the bottom of the pores. When the reaction is very fast, i.e. $k \to \infty$, the limiting current I_s becomes equal to I_{Ds}, as given by Eq. (14). This represents the diffusion limiting current for a reversible reaction at a recessed electrode. From Eqs. (14) and (20), the intercept of the K–L plots at $\omega \to \infty$, I_{ks}, is given by:

$$\frac{1}{I_{ks}}=\frac{1}{I_k}+\frac{1}{I_s}=-\frac{1}{nFA_s k(E)c^b}-\frac{d_{eff}}{nFA_s Dc^b} \quad (21)$$

I_{ks} replaces the kinetic term I_k for an activated electron transfer reaction at an unblocked electrode [19] and shows that the limiting current at $\omega\to\infty$ contains a contribution due to the electrode geometry. For an irreversible electron transfer reaction at an unblocked electrode, the limiting current is given by [19]:

$$\frac{1}{I}=\frac{1}{I_k}+\frac{1}{I_D}=-\frac{1}{nFAc^b k}-\frac{\delta}{nFADc^b} \quad (22)$$

For the analysis of the kinetics of the electron transfer reaction at an unblocked electrode, it is convenient to express Eq. (22) in terms of a current function of the type [19]:

$$\log\left(\left|\frac{I\times I_D}{I_D-I}\right|\right)=\log(nFAc^b k^0)-\frac{\alpha nf}{2.303}(E-E^0) \quad (23)$$

From Eq. (20), $1/I=1/I_k+1/I_{Ds}$, it is easy to show that, for a recessed electrode, Eq. (23) takes the form:

$$\log\left(\left|\frac{I\times I_{Ds}}{I_{Ds}-I}\right|\right)=\log(nFA_s c^b k^0)-\frac{\alpha nf}{2.303}(E-E^0) \quad (24)$$

A comparison of Eqs. (23) and (24) show that the potential dependence of the current function for the recessed electrode case is the same as for an unblocked electrode when the value of the diffusion limiting current is used. The difference between these two current functions yields A_s/A and hence, ϕ.

In conclusion, Eqs. (20) and (22) show that the inverse of the limiting current extrapolated to infinite rotation rate for a blocked recessed electrode should have a potential dependent limiting intercept and reach a constant value at very negative potentials given by:

$$\lim_{k\to\infty}\frac{1}{I_{ks}}=\frac{1}{I_s}=-\frac{d_{eff}}{nFA_s Dc^b}=-\frac{d_{eff}}{nF(1-\phi)ADc^b} \quad (25)$$

This limiting value will depend on the geometry of the electrode surface (see Eq. (21)).

3. Experimental

The validity of the equations derived above was tested at a RDE of 0.14 cm radius using a fast reversible reaction, the reduction of hexacyanoferrate(III), and an irreversible reaction, the reduction of oxygen, as examples. The experiments were performed in 0.1 M KOH in a three-electrode cell with a Pt counter electrode and a Ag | AgCl | KCl (sat) reference electrode. All potentials are referred to this electrode.

The porous blocking film employed was nickel hydroxide electrochemically deposited on a Pt electrode under conditions where a porous film is formed. The film was electrodeposited from a deaerated 0.1 M $Ni(NO_3)_2$ solution, according to the method of Gonsalves and Hillman [21]. The potential was swept from 40 to −640 mV at a sweep rate of 10 mV s^{-1} and held at this potential for 180 s. Hydrogen evolution causes a local increase in pH at the electrode surface and hence precipitation of $Ni(OH)_2$. The potential was swept back to 40 mV and the electrode was finally rinsed with doubly distilled water. The thickness of the film was determined after the RDE experiments by scanning its surface with a profilometer (Mitotoyo SV502) over the edge created by partial removal of the film from the surface.

All chemicals were of AnalaR grade and were used as received; all experiments were carried out at room temperature 22±2 °C.

4. Results and discussion

4.1. Koutecký–Levich plots analysis

Figs. 5 and 6 compare the RDE results for oxygen reduction on bare Pt and on Pt covered with a 0.5 μm layer of $Ni(OH)_2$. The potential was initially swept from the positive to the negative limit at a sweep rate of 10 mV s^{-1} and the results shown correspond to currents measured during the subsequent positive going sweep. This procedure was adopted to avoid kinetic complications resulting from slow reduction of platinum oxide. The $Ni(OH)_2$ film was electrochemically inactive in the potential region investigated. A comparison of the results in these two figures show that the electrochemical response on the porous electrode is similar to that of the Pt substrate, the main difference being the lower currents observed for the porous electrode. Similar results were obtained for 5 mM $K_3Fe(CN)_6$ in 0.1 M KOH for both electrodes.

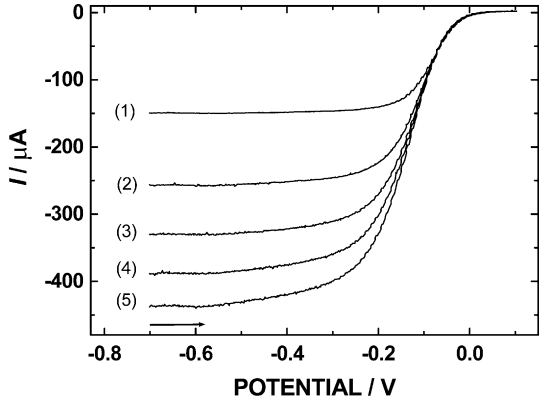

Fig. 5. Dependence of current on potential for the reduction of oxygen in O_2 saturated 0.1 M KOH on a rotating disc Pt electrode. Rotation rates: (1) 300; (2) 900; (3) 1500; (4) 2100 and (5) 2700 rpm.

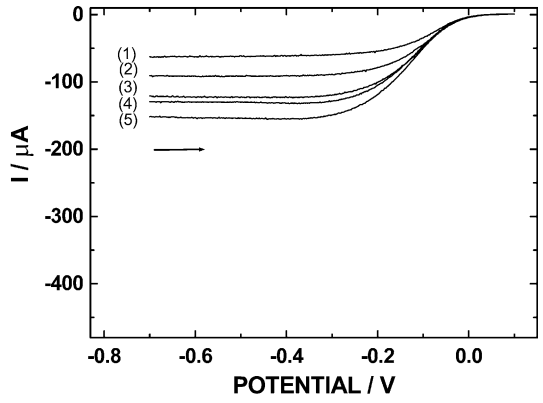

Fig. 6. Dependence of current on potential for the reduction of oxygen in O_2 saturated 0.1 M KOH on a rotating disc Pt electrode covered with a 0.5 μm layer of $Ni(OH)_2$. Rotation rates: (1) 100; (2) 300; (3) 900; (4) 1500 and (5) 2700 rpm.

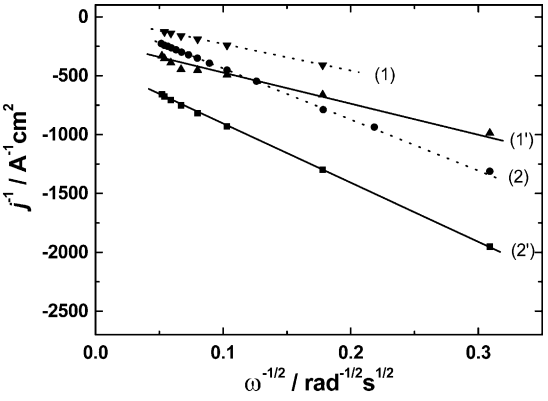

Fig. 7. Koutecký–Levich plots in the limiting current region for 5 mM hexacyanoferrate(III) and O_2 saturated solutions on an unblocked Pt electrode (lines (1) and (2)), and on a porous $Pt/Ni(OH)_2$ electrode (lines (1′) and (2′)). The base electrolyte was 0.1 M KOH.

Fig. 7 shows a comparison of the K–L plots of the diffusionally controlled currents for the two electrochemical reactions studied at the unblocked and porous electrodes, respectively. For the Pt electrode, j^{-1} extrapolates to zero when $\omega \to \infty$, as expected for a diffusionally controlled reaction. The corresponding extrapolation for the reduction of Fe(III) and O_2 on the porous electrode was 412 ± 4 and 243 ± 15 A^{-1} cm^2, respectively. (These current densities are reported per unit of geometrical area.)

The calculation of $d_{\text{eff}}/(1-\phi)$ from Eq. (25) requires the values of the diffusion coefficients. For hexacyanoferrate(III), this was calculated from the Levich equation in the limiting current region and a value of $D_{\text{Fe(III)}} = (6.81 \pm 0.04) \times 10^{-6}$ cm^2 s^{-1} was obtained. This result is in agreement with that calculated from Ref. [22]. $D_{\text{Fe(III)}}$ was obtained by recalculation of the temperature coefficient of the diffusion coefficient data at different concentrations of KOH given in this reference and a value of $D_{\text{Fe(III)}} = (6.82 \pm 0.04) \times 10^{-6}$ cm^2 s^{-1} at 22 °C was found. For oxygen, the diffusion coefficient was calculated from Ref. [23] considering the Einstein–Stokes relationship $D\eta/T = \text{constant}$, where η is the viscosity [24]. The ratio of viscosity for 0.1 M KOH between 25 and 22 °C was taken to be the same as that for pure water [25]. With these assumptions, $D_{O_2} = 1.73 \times 10^{-5}$ cm^2 s^{-1} at 22 °C. The oxygen concentration was calculated from Ref. [12] considering that the ratio of O_2 solubility between different temperatures is independent of KOH concentration. The solubility of O_2 in water was taken from Ref. [25] and a value of $c^{b}_{O_2} = 1.29 \times 10^{-6}$ mol cm^{-3} was found.

The results obtained are collected in Table 1. The only parameter that can be calculated from the K–L plots, $d_{\text{eff}}/(1-\phi)$, combines the effective diffusional path through the film, its porosity and the inhomogeneity of the diffusional geometry at the pore entrances. Therefore, the limiting current gives only a partial description of diffusion across a recessed porous film electrode. If d is taken as the geometrical film thickness and pore entrance effects are ignored, blocking factors of 0.963 and 0.976 can be calculated.

The limiting current observed (compare Figs. 5 and 6) is a consequence of the porous nature of the surface. A simple way to test for the presence of this electrode geometry is to combine Eq. (14) with the Levich equation for the Pt electrode (i.e. when $d_{\text{eff}} = 0$). At sufficiently negative potentials the ratio of currents at the Pt and the $Pt/Ni(OH)_2$ electrodes are given by:

$$\frac{I_{\text{Pt}}}{I_{\text{Pt/Ni(OH)}_2}} = 1 + \frac{d_{\text{eff}}}{1.61 D^{1/3} \upsilon^{1/6}} \frac{A}{A_s} \omega^{1/2} = 1 + \frac{d_{\text{eff}}}{1.61 D^{1/3} \upsilon^{1/6} (1-\phi)} \omega^{1/2} \quad (26)$$

A test of Eq. (26) is shown in Fig. 8. A linear dependence of the current ratio is observed and these values extrapolate to unity for $\omega \to 0$, as predicted from Eq. (26). Although no new information can be obtained, the use of Eq. (26) tests the applicability of the analysis described in this paper to experimental data. Values of $d_{\text{eff}}/(1-\phi)$ of 14 and 20 μm were calculated for the reduction of Fe(III) and O_2. There are no major differences between these values and those calculated from the limiting current from the K–L plots although these two methods give different weightings to the data. Eq. (25) requires an extrapolation of j^{-1} to $\omega^{-1/2} \to 0$ whereas Eq. (26) uses the data sets directly.

4.2. Current function analysis

The comparison of the potential dependence of the current functions given by Eqs. (23) and (24) for the two electrode surfaces investigated can provide additional information on the mass transport through the film. The

Table 1
Porosity parameters and tortuosity factors for the reduction of hexacyanoferrate(III) and oxygen on the Pt/$Ni(OH)_2$ film electrode

Reaction	$d_{eff}/(1-\phi)$/cm [a]	ϕ [b]	ϕ [c]	d_{eff}/cm [d]	θ_t [e]	θ_t [f]	θ_t [g]
Hexacyanoferrate(III)	1.36×10^{-3}	0.963	0.74	3.5×10^{-4}	2.7	6.7	3.8
O_2	2.09×10^{-3}	0.976	0.75	5.2×10^{-4}	3.2	7.0	4.0

[a] Calculated from K–L plots, Fig. 7.
[b] Calculated assuming $d = 5 \times 10^{-5}$ cm and $\Sigma = 0$ for the K–L results.
[c] Calculated from the current function analysis, Eqs. (23) and (24).
[d] Calculated from the current function and Eq. (25).
[e] Calculated using d_{eff} from the current function, $d = 5 \times 10^{-5}$ cm and $\Sigma = 0$.
[f] Calculated from Eq. (30).
[g] Calculated from Eq. (31).

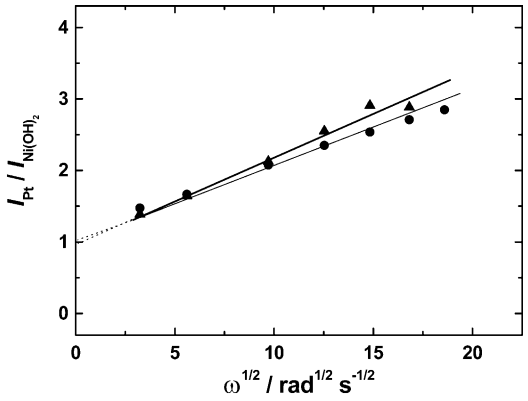

Fig. 8. Test of Eq. (26) for the reduction of hexacyanoferrate(III) (●) and oxygen (▲) on Pt and Pt/$Ni(OH)_2$ electrodes.

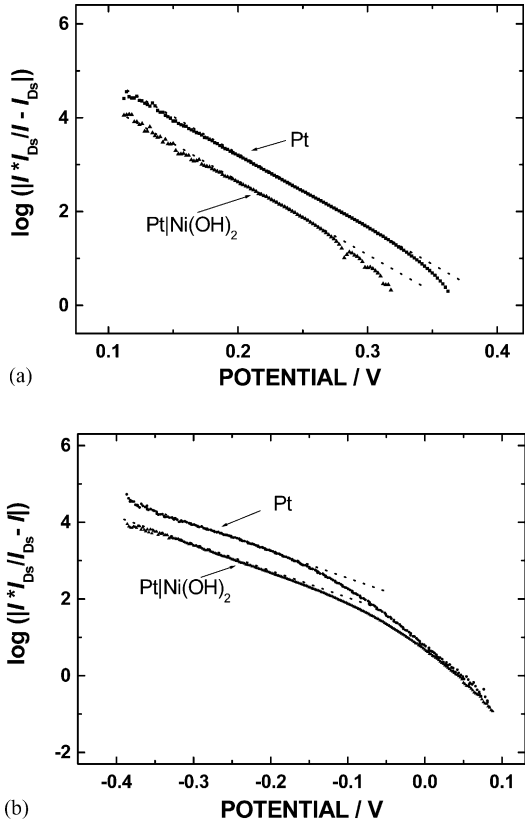

Fig. 9. Comparison of the potential dependence of the current functions from Eqs. (23) and (24) for the reduction of hexacyanoferrate(III) (a) and oxygen (b) in 0.1 M KOH on an unblocked and a Pt electrode blocked with a 0.5 μm film of $Ni(OH)_2$. The current function values are the average for the rotation rates measured.

$Ni(OH)_2$ film is electrochemically inert in the potential range investigated (results not shown) and therefore reduction is expected to take place at the bottom of the pores. Fig. 9a and b compare the potential dependence of the current function for the blocked and unblocked electrodes. For potentials more negative than −0.2 V the current functions are lower on the blocked electrode by factors of approximately 3.7 and 4 for the Fe(III) and O_2 reduction reactions. From Eqs. (23) and (24), this corresponds to ratios A_s/A of 0.27 and 0.25, respectively, and hence, to an average value of the blocking factor $\phi = 0.74$ (Table 1).

At first sight, it might seem surprising that, in spite of the small fraction of unblocked surface available for reaction, comparative high limiting currents are observed (e.g., compare Figs. 5 and 6). The reason for this is the small value of d (5×10^{-5} cm) in comparison with δ. It must be noted that Eq. (25) predicts a finite value I_s for the limiting current when both $\omega \to \infty$ and $k \to \infty$ whereas an unblocked electrode would lead to $I_s \to \infty$. In the absence of information on surface geometry, however, the wrong value of the rate constant and indeed of the reduction mechanism would be derived from measurements of the polarisation curves.

4.3. The effective diffusional length and tortuosity coefficients

The large difference between the values of ϕ derived from the current function results (Fig. 9a and b) and those calculated from the K–L plots is due to the different features probed by these two methods for calculating the ratio A_s/A. When using I_{ks}^{-1}, both the diffusional length and the diffusion coefficient within the film determine A_s. In this case, tortuosity effects

within the film and a finite value of Σ will increase the calculated value of ϕ. On the other hand, when the current functions are used (Eqs. (23) and (24)), the comparison is now based on the value of the product of the area by the standard rate constant, and importantly, the diffusional length within the pore does not influence the potential dependence of the current function. Thus, the value of ϕ calculated is independent of the diffusion coefficients within the film pores on the assumption that reduction of O_2 and Fe(III) does not take place on $Ni(OH)_2$.

Diffusion through porous media has been analysed considering an effective diffusion coefficient D_{eff} given by [26,27]:

$$D_{eff} = \frac{1-\phi}{\theta_t^2} D_0 \tag{27}$$

where the tortuosity coefficient, θ_t, is the ratio of the mean increase in diffusional path per unit length in the direction of diffusion within the material, and D_0 is the diffusion coefficient in the solution bulk. This way of treating diffusional mass transfer through porous media preserves the form of the steady state diffusion equation as [28]:

$$\text{Flux density} = -D_{eff}\frac{\Delta c}{d} \tag{28}$$

Δc is the concentration difference across the porous material and d its thickness. From Eq. (27), the effective diffusional length becomes:

$$d_{eff} = \theta_t^2 d + (1-\phi)\Sigma \tag{29}$$

when both tortuosity and pore entrance effects are taken into account.

The blocking factor found from the current function analysis, $\phi = 0.74$, can be used to calculate d_{eff} from the limiting value of I_{ks} (Eq. (25)). The values obtained are shown in Table 1. Since ϕ obtained from the current function analysis does not depend on the diffusional path length, this value can be combined with that of $d_{eff}/(1-\phi)$ obtained from the K–L plots to estimate θ_t. If the term $(1-\phi)\Sigma$ is much less than d (see justification for this later on), i.e. the film tortuosity dominates the effective diffusional length within the film, tortuosity coefficients comprised between 2.7 and 3.2 are calculated.

The origin of the difference in θ_t calculated from the Fe(III) and the O_2 data is unclear. Since the hexacyanoferrate anions are much bigger than the O_2 molecule, results for this couple would have been expected to yield a larger value of θ_t either through an increased diffusional path or due to a decrease in the value of the diffusion coefficient for the species in the pores. For oxygen, reduction to water has been assumed but if $n = 2$, the value of θ_t calculated would be less than that for the Fe(III) experiments. Since the limiting cathodic currents have been employed in the calculations, it is very unlikely that the reduction would stop at the peroxide stage. Further work is in progress to elucidate this point. Indeed, if the film displays ion exchange properties, the concentration that would need to be used in Eq. (14) would be different from the bulk value.

Using a simple model, Mackie and Meares proposed that the tortuosity coefficient is given by [29]:

$$\theta_t = \frac{1+v_S}{1-v_S} \tag{30}$$

where v_S is the volume fraction occupied by the solid phase of the porous material. This relationship has been extensively used for the analysis of transport phenomena through membranes [29–34]. θ_t has also been calculated using a random film model to give [34]:

$$\theta_t = \frac{1}{1-v_S} \tag{31}$$

From the definition of the blocking factor, $\phi = (A - A_s)/A$, it can be seen that $v_S = \phi$. The tortuosity coefficients calculated from the blocking factor are compared with model calculations in Table 1. Eq. (30) appears to be in better agreement with the results for hexacyanoferrate(III) but the data for oxygen gives a higher value of θ_t.

Unfortunately, it is not possible to separate the tortuosity from Σ unless separate measurements on θ_t are made and usually this coefficient is employed as an adjustable parameter in the analysis of diffusion in porous media. However, it is possible to assess the upper bound of the contribution of Σ to the diffusional path d_{eff} (Eq. (29)). Landsberg and co-workers observed that the transition from a regime where $\delta > r_2$ to $\delta < r_2$ was characterised by a change in the slope of the K–L plot at $\delta = r_2$ [13,15] and used this feature to calculate the blocking factor. No such change in slope was observed in the present work up to a rotation rate of 3600 rpm. At this rotation rate, from Eq. (1), $\delta = 2.3 \times 10^{-4}$ cm for the Fe(III) solution and hence, $r_2 < 2.3 \times 10^{-4}$ cm. Since $\Gamma_{pore} = 1/\pi r_2^2$, a minimum pore density value of 6×10^6 pores cm^{-2} can be estimated for the film electrode used. This value also fixes an upper bound for the parameter Σ. For a blocking factor of the order of 0.75, a value of $\Sigma < 1.1 \times 10^{-4}$ cm is calculated from Eq. (17), which leads to a maximum contribution of pore entrance effects to d_{eff} of less than 2.7×10^{-5} cm, i.e. its contribution is 5 to 10 times smaller than that due to tortuosity effects. In conclusion, the effect of non-linear diffusion at the pore entrances is overshadowed by the tortuosity of the nickel hydroxide layer.

The purpose of this work was not to measure the kinetics of oxygen reduction under oxide films and for this reason, a full kinetic analysis is not presented here.

The results for potentials more positive than −0.15 V, however, deserve mention. For the bare Pt electrode a Tafel slope of approximately 60 mV decade^{-1} is observed. Surprisingly, the reduction currents on the $Ni(OH)_2$ covered electrode are very similar to those for Pt as the potential is made more positive (Fig. 9b). This is only possible if the rate constant for oxygen reduction in this potential region is larger on the covered electrode compared with bare Pt. It is proposed that it originates from the electrocatalytic properties of nickel hydroxide. In the absence of oxygen, $Ni(OH)_2$ is stable in the potential range −0.1 to 0.4 V; NiO(OH) formation and reduction occurs at more positive potentials (data not shown). However, in the presence of oxygen, chemical oxidation of $Ni(OH)_2$ by O_2 can result in the formation of the nickel oxy-hydroxide which is electrochemically reduced to provide a redox catalytic cycle reduction channel and hence, an increase in the reduction current and in the value of the Tafel slope. Similar effects have been previously observed for the reduction of H_2O_2 on copper [35]. At potentials more negative than −0.1 V, the reduction takes place directly on the exposed Pt surface and no current enhancement due to the oxide film is apparent.

5. Conclusions

The case of a partially blocked recessed RDE has been analysed. An approximate solution, based on the analogy of the differential equations of diffusion and electrical conduction has been presented. The results show that great care has to be taken when analysing the kinetics of electrochemical reactions for inhomogeneous electrodes since the apparent values of rate constants derived from RDE experiments contain contributions not only due to partial blocking of the surface but also, importantly, from its geometry. This is an important consideration when carrying out electron transfer kinetic studies for electrodes covered by a porous layer. It is shown that a comparison of the potential dependence of the current function $\log(|(I \times I_{Ds})/(I_{Ds}-I)|)$ (Eq. (24)) with the limiting currents for the Koutecký–Levich plots can yield additional information on the nature of the porous layer, but tortuosity effects cannot be deconvoluted from the inhomogeneity of the diffusional field close to the pores entrance.

Acknowledgements

The support of the European Union, CLETEPEG project (Contract No: G5RD-CT-2001-00-463, Growth Programme) is gratefully acknowledged.

References

[1] B.R. Scharifker, J. Electroanal. Chem. 240 (1988) 61.
[2] R.M. Penner, C.R. Martins, Anal. Chem. 59 (1987) 2652.
[3] K.J. Vetter, Z. Physik. Chim. 199 (1952) 19.
[4] H.J. Lee, C. Beriet, R. Ferrigno, H.H. Girault, J. Electroanal. Chem. 502 (2001) 138.
[5] C. Amatore, J.M. Savéant, D. Tessier, J. Electroanal. Chem. 147 (1983) 39.
[6] F.A. Armstrong, A.M. Bond, H.A.O. Hill, I.S.M. Psalti, C.G. Zoski, J. Phys. Chem. 93 (1989) 6485.
[7] F.A. Armstrong, A.M. Bond, H.A.O. Hill, B.N. Oliver, I.S.M. Psalti, J. Am. Chem. Soc. 111 (1989) 9185.
[8] T. Gueshi, K. Tokuda, J. Matsuda, J. Electroanal. Chem. 89 (1978) 247.
[9] J. Lindemann, R. Landsberg, J. Electroanal. Chem. 30 (1971) 79.
[10] J. Lindemann, R. Landsberg, J. Electroanal. Chem. 31 (1971) 107.
[11] R. Landsberg, R. Thiele, Electrochim. Acta 11 (1966) 1243.
[12] F. Scheller, R. Landsberg, S. Müller, J. Electroanal. Chem. 20 (1969) 375.
[13] F. Scheller, S. Müller, R. Landsberg, J.-J. Spitzer, J. Electroanal. Chem. 19 (1968) 187.
[14] C. Deslouis, B. Tribollet, M. Duprat, F. Moran, J. Electrochem. Soc. 134 (1987) 2496.
[15] F. Scheller, R. Landsberg, H. Wolf, Electrochim. Acta 15 (1970) 525.
[16] W.R. Smythe, J. Appl. Phys. 24 (1953) 70.
[17] E. Levart, D. Schuhmann, O. Contamin, J. Electroanal. Chem. 70 (1976) 117.
[18] R. Ferrigno, P.-F. Brevet, H.H. Girault, J. Electroanal. Chem. 430 (1997) 235.
[19] A.J. Bard, L. Faulkner, Electrochemical Methods, Wiley, New York, 2001.
[20] MICROCAL ORIGIN software, version 6.0.
[21] M. Gonsalves, A. Robert Hillman, J. Electroanal. Chem. 454 (1998) 183.
[22] A.J. Arvía, S.L. Marchiano, J.J. Podesta, Electrochim. Acta 12 (1967) 259.
[23] R.E. Davis, G.L. Horvath, C.W. Tobias, Electrochim. Acta 12 (1967) 287.
[24] R.A. Robinson, R.H. Stokes, Electrolyte Solutions, Butterworths Scientific Publications, London, 1959, p. 12.
[25] D.R. Lide, CRC Handbook of Chemistry and Physics, 82nd ed., CRC Press, Boca Raton, Florida, USA, 2001.
[26] E.S. Cussler, Diffusion: Mass Transfer in Fluid Systems, Cambridge University Press, Cambridge, 1984, p. 185.
[27] M. Higa, A. Kira, J. Phys. Chem. 98 (1994) 6339.
[28] A.H. Muhr, J.M. Blanshard, Polymer 23 (1984) 1012.
[29] J.S. Mackie, P. Meares, Proc. R. Soc. Lond. A 232 (1955) 498.
[30] D. Mackay, J. Phys. Chem. 64 (1960) 1718.
[31] A.A. Jenkins, W.C. Maskell, F.L. Tye, J. Chem. Soc. Faraday Trans. 89 (1993) 3427.
[32] P. Meares, J. Chim. Phys. 55 (1958) 273.
[33] H. Ferguson, C.R. Gardner, R. Paterson, J. Chem. Soc. Faraday Trans. 1 89 (1972) 2021.
[34] J.A. Lee, W.C. Maskell, F.L. Tye, in: P. Meares (Ed.), Membrane Separation Processes (Chapter 11), Elsevier, Amsterdam, 1976, p. 400.
[35] M.V. Vazquez, S.R. Sanchez, E.J. Calvo, D.J. Schiffrin, J. Electroanal. Chem. 179 (1994) 187.